iPSCs can be differentiated into the affected cell types or tissues, allowing direct functional assays to be performed that are associated with the pathology. Second, because the disease-causing potential of some mutations is dependent on the genetic backgrounds of the patients,[38] it may be better to obtain both mutant and wild-type clones from a single mosaic patient to more accurately assess the impact of the mutation(s).

Considering that a mutation of *NLRP3* in 10% of the cells is sufficient to cause a distinct disease phenotype, somatic mutations of various genes at an even rarer frequency may also affect the biologic characteristics of a person. Because the presence of the *NLRP3* mutation did not affect the efficacy of reprogramming to the iPSCs, we may be able to obtain both mutant and wild-type iPSC clones from CINCA syndrome patients who carry *NLRP3* mutant cells at a lower percentage. In some diseases, such as Fanconi anemia, however, mutant cells may be resistant to reprogramming.[39,40] Even though there are some possible limitations, establishing both mutant and wild-type iPSC clones is a promising approach to dissect the extent and role of somatic mosaicism.

We demonstrated that several inhibitors that are considered to be effective against CINCA syndrome actually attenuated the disease-relevant phenotype of iPSC-derived macrophages. Before a successful drug screening using iPSC-derived somatic cells can be developed, several limitations need to be overcome, such as the heterogeneity of differentiation and difficulties associated with purification.[18] In this report, we used an efficient and robust differentiation protocol and obtained plenty of macrophages free from the clonal variations.

In conclusion, we elucidated the pathologic roles of both mutant and wild-type cells in mosaic CINCA syndrome patients. After obtaining iPSC-derived macrophages in large quantity and with high purity, we showed they are applicable for drug screening. The iPSC-based approach may help to illuminate the pathogenesis of various diseases that are caused by somatic mosaicism, and facilitate drug discovery for the treatment of NLRP3-related inflammatory diseases.

Acknowledgments

The authors thank the CINCA syndrome patients who participated in this study; Y. Sasaki, Y. Jindai, A. Okada, M. Narita, A. Nagahashi, T. Ohkame, S. Nishimoto, Y. Inoue, and S. Arai for technical assistance; I. Kato for help with animal experiments; M. Nakagawa, K. Okita, Y. Yoshida, T. Aoi, and M. Yanagimachi for scientific comments; and R. Kato, E. Nishikawa, S. Takeshima, Y. Otsu, H. Hasaba, H. Watanabe, T. Ishii, H. Kurokawa, N. Takasu, and Y. Takao for administrative assistance.

This work was supported by the Ministry of Health, Labor and Welfare (N.M. and T.N.), the Ministry of Education, Culture, Sports, Science and Technology (MEXT; N.M. and T.N.), the Leading Project of MEXT (S.Y. and T.N.), the Promotion of Fundamental Studies in Health Sciences of National Institute of Biomedical Innovation (S.Y.), the Funding Program for World-Leading Innovative Research and Development on Science and Technology (FIRST Program) of Japan Society for the Promotion of Science (JSPS; T.N., and S.Y.), JSPS and MEXT (Grants-in-Aid for Scientific Research; S.Y.), JSPS (T.N., T.T., and M.K.S.), the Takeda Science Foundation, SENSHIN Medical Research Foundation, and Suzuken Memorial Foundation to (M.K.S.).

Authorship

Contribution: T.T. planned the project, established iPSCs, performed experimental work, analyzed data, and prepared the manuscript; K.T. planned the project, established iPSCs, and analyzed data; M.Y., S.T., and S.N. performed experimental work; K.O., A.N., and T.H. analyzed data; R.N. and N.K. planned the project; H.H. and M.M. performed *L monocytogenes* infection; N.M. and J.E.H. performed electron microscopy; T.Y. identified retroviral integration sites; A.W. performed bisulfite sequencing; A.S.-O. and S.O. analyzed CNV; I.A. established iPSCs; S.Y. and T.N. planned the project and analyzed data; M.K.S. planned the project, analyzed data, and prepared the manuscript; and all authors read and approved the manuscript.

Conflict-of-interest disclosure: S.Y. is a member without salary of the scientific advisory boards of iPierian, iPS Academia Japan, and Megakaryon Corporation. The remaining authors declare no competing financial interests.

Correspondence: Megumu K. Saito, Center for iPS Cell Research and Application, Kyoto University, Kyoto 606-8507, Japan; e-mail: msaito@cira.kyoto-u.ac.jp.

References

1. Prieur AM, Griscelli C, Lampert F, et al. A chronic, infantile, neurological, cutaneous and articular (CINCA) syndrome: a specific entity analysed in 30 patients. *Scand J Rheumatol Suppl.* 1987;66:57-68.
2. Aksentijevich I, Nowak M, Mallah M, et al. De novo CIAS1 mutations, cytokine activation, and evidence for genetic heterogeneity in patients with neonatal-onset multisystem inflammatory disease (NOMID): a new member of the expanding family of pyrin-associated autoinflammatory diseases. *Arthritis Rheum.* 2002;46(12):3340-3348.
3. Feldmann J, Prieur AM, Quartier P, et al. Chronic infantile neurological cutaneous and articular syndrome is caused by mutations in CIAS1, a gene highly expressed in polymorphonuclear cells and chondrocytes. *Am J Hum Genet.* 2002;71(1):198-203.
4. Bauernfeind FG, Horvath G, Stutz A, et al. Cutting edge: NF-kappaB activating pattern recognition and cytokine receptors license NLRP3 inflammasome activation by regulating NLRP3 expression. *J Immunol.* 2009;183(2):787-791.
5. Mariathasan S, Weiss DS, Newton K, et al. Cryopyrin activates the inflammasome in response to toxins and ATP. *Nature.* 2006;440(7081):228-232.
6. Gattorno M, Tassi S, Carta S, et al. Pattern of interleukin-1beta secretion in response to lipopolysaccharide and ATP before and after interleukin-1 blockade in patients with CIAS1 mutations. *Arthritis Rheum.* 2007;56(9):3138-3148.
7. Goldbach-Mansky R, Dailey NJ, Canna SW, et al. Neonatal-onset multisystem inflammatory disease responsive to interleukin-1beta inhibition. *N Engl J Med.* 2006;355(6):581-592.
8. Neven B, Marvillet I, Terrada C, et al. Long-term efficacy of the interleukin-1 receptor antagonist anakinra in ten patients with neonatal-onset multisystem inflammatory disease/chronic infantile neurologic, cutaneous, articular syndrome. *Arthritis Rheum.* 2010;62(1):258-267.
9. Saito M, Nishikomori R, Kambe N, et al. Disease-associated CIAS1 mutations induce monocyte death, revealing low-level mosaicism in mutation-negative cryopyrin-associated periodic syndrome patients. *Blood.* 2008;111(4):2132-2141.
10. Tanaka N, Izawa K, Saito MK, et al. High incidence of NLRP3 somatic mosaicism in patients with chronic infantile neurologic, cutaneous, articular syndrome: results of an International Multicenter Collaborative Study. *Arthritis Rheum.* 2011;63(11):3625-3632.
11. Masters SL, Simon A, Aksentijevich I, Kastner DL. Horror autoinflammaticus: the molecular pathophysiology of autoinflammatory disease. *Annu Rev Immunol.* 2009;27:621-668.
12. Youssoufian H, Pyeritz RE. Mechanisms and consequences of somatic mosaicism in humans. *Nat Rev Genet.* 2002;3(10):748-758.
13. Erickson RP. Somatic gene mutation and human disease other than cancer: an update. *Mutat Res.* 2010;705(2):96-106.
14. Ariga T, Kondoh T, Yamaguchi K, et al. Spontaneous in vivo reversion of an inherited mutation in the Wiskott-Aldrich syndrome. *J Immunol.* 2001;166(8):5245-5249.

15. Nishikomori R, Akutagawa H, Maruyama K, et al. X-linked ectodermal dysplasia and immunodeficiency caused by reversion mosaicism of NEMO reveals a critical role for NEMO in human T-cell development and/or survival. *Blood.* 2004; 103(12):4565-4572.
16. Lutskiy MI, Beardsley DS, Rosen FS, Remold-O'Donnell E. Mosaicism of NK cells in a patient with Wiskott-Aldrich syndrome. *Blood.* 2005;106(8):2815-2817.
17. Takahashi K, Tanabe K, Ohnuki M, et al. Induction of pluripotent stem cells from adult human fibroblasts by defined factors. *Cell.* 2007;131(5): 861-872.
18. Grskovic M, Javaherian A, Strulovici B, Daley GQ. Induced pluripotent stem cells: opportunities for disease modelling and drug discovery. *Nat Rev Drug Discov.* 2011;10(12):915-929.
19. Hanna J, Markoulaki S, Schorderet P, et al. Direct reprogramming of terminally differentiated mature B lymphocytes to pluripotency. *Cell.* 2008;133(2): 250-264.
20. Saito M, Fujisawa A, Nishikomori R, et al. Somatic mosaicism of CIAS1 in a patient with chronic infantile neurologic, cutaneous, articular syndrome. *Arthritis Rheum.* 2005;52(11):3579-3585.
21. Nakano T, Kodama H, Honjo T. Generation of lymphohematopoietic cells from embryonic stem cells in culture. *Science.* 1994;265(5175):1098-1101.
22. Fujisawa A, Kambe N, Saito M, et al. Disease-associated mutations in CIAS1 induce cathepsin B-dependent rapid cell death of human THP-1 monocytic cells. *Blood.* 2007;109(7):2903-2911.
23. Willingham SB, Bergstralh DT, O'Connor W, et al. Microbial pathogen-induced necrotic cell death mediated by the inflammasome components CIAS1/cryopyrin/NLRP3 and ASC. *Cell Host Microbe.* 2007;2(3):147-159.
24. Iyer SS, Pulskens WP, Sadler JJ, et al. Necrotic cells trigger a sterile inflammatory response through the Nlrp3 inflammasome. *Proc Natl Acad Sci U S A.* 2009;106(48):20388-20393.
25. Beigi RD, Kertesy SB, Aquilina G, Dubyak GR. Oxidized ATP (oATP) attenuates proinflammatory signaling via P2 receptor-independent mechanisms. *Br J Pharmacol.* 2003;140(3):507-519.
26. Martinon F, Petrilli V, Mayor A, Tardivel A, Tschopp J. Gout-associated uric acid crystals activate the NALP3 inflammasome. *Nature.* 2006; 440(7081):237-241.
27. Halle A, Hornung V, Petzold GC, et al. The NALP3 inflammasome is involved in the innate immune response to amyloid-beta. *Nat Immunol.* 2008;9(8):857-865.
28. Duewell P, Kono H, Rayner KJ, et al. NLRP3 inflammasomes are required for atherogenesis and activated by cholesterol crystals. *Nature.* 2010; 464(7293):1357-1361.
29. Masters SL, Dunne A, Subramanian SL, et al. Activation of the NLRP3 inflammasome by islet amyloid polypeptide provides a mechanism for enhanced IL-1beta in type 2 diabetes. *Nat Immunol.* 2010;11(10):897-904.
30. Vandanmagsar B, Youm YH, Ravussin A, et al. The NLRP3 inflammasome instigates obesity-induced inflammation and insulin resistance. *Nat Med.* 2011;17(2):179-188.
31. Juliana C, Fernandes-Alnemri T, Wu J, et al. Anti-inflammatory compounds parthenolide and Bay 11-7082 are direct inhibitors of the inflammasome. *J Biol Chem.* 2010;285(13):9792-9802.
32. Aizawa E, Hirabayashi Y, Iwanaga Y, et al. Efficient and accurate homologous recombination in hESCs and hiPSCs using helper-dependent adenoviral vectors. *Mol Ther.* 2012;20(2):424-431.
33. Soldner F, Laganiere J, Cheng AW, et al. Generation of isogenic pluripotent stem cells differing exclusively at two early onset Parkinson point mutations. *Cell.* 2011;146(2):318-331.
34. Cheung AY, Horvath LM, Grafodatskaya D, et al. Isolation of MECP2-null Rett syndrome patient hiPS cells and isogenic controls through X-chromosome inactivation. *Hum Mol Genet.* 2011;20(11):2103-2115.
35. Kim KY, Hysolli E, Park IH. Neuronal maturation defect in induced pluripotent stem cells from patients with Rett syndrome. *Proc Natl Acad Sci U S A.* 2011;108(34):14169-14174.
36. Pomp O, Dreesen O, Leong DF, et al. Unexpected X chromosome skewing during culture and reprogramming of human somatic cells can be alleviated by exogenous telomerase. *Cell Stem Cell.* 2011;9(2):156-165.
37. Gore A, Li Z, Fung HL, et al. Somatic coding mutations in human induced pluripotent stem cells. *Nature.* 2011;471(7336):63-67.
38. Crotti L, Lundquist AL, Insolia R, et al. KCNH2-K897T is a genetic modifier of latent congenital long-QT syndrome. *Circulation.* 2005;112(9): 1251-1258.
39. Raya A, Rodriguez-Piza I, Guenechea G, et al. Disease-corrected haematopoietic progenitors from Fanconi anemia induced pluripotent stem cells. *Nature.* 2009;460(7251):53-59.
40. Müller LU, Milsom MD, Harris CE, et al. Overcoming reprogramming resistance of Fanconi anemia cells. *Blood.* 2012;119(23):5449-5457.

DNA Research 19, 143–152, (2012)
Advance Access Publication on 24 January 2012
doi:10.1093/dnares/dsr047

Detection of Base Substitution-Type Somatic Mosaicism of the *NLRP3* Gene with >99.9% Statistical Confidence by Massively Parallel Sequencing

Kazushi Izawa[1,†], Atsushi Hijikata[2,†], Naoko Tanaka[1], Tomoki Kawai[1], Megumu K Saito[3], Raphaela Goldbach-Mansky[4], Ivona Aksentijevich[5], Takahiro Yasumi[1], Tatsutoshi Nakahata[3], Toshio Heike[1], Ryuta Nishikomori[1,*], and Osamu Ohara[2,6,*]

Department of Pediatrics, Kyoto University Graduate School of Medicine, 54 Shogoin Sakyo, Kyoto 606-8507, Japan[1]; Laboratory for Immunogenomics, RIKEN Research Center for Allergy and Immunology, RIKEN Yokohama Institute, 1-7-22 Suehiro-cho Tarumi-ku, Yokohama, Kanagawa 230-0045, Japan[2]; Clinical Application Department, Center for iPS Cell Research and Application (CiRA), Kyoto University, Kyoto, Japan[3]; Translational Autoinflammatory Disease Section NIH/NIAMS, Bethesda, MD, USA[4]; The National Human Genome Research Institute, Bethesda, MD, USA[5] and Department of Human Genome Research, Kazusa DNA Research Institute, 2-6-7 Kazusa-kamatari, Kisarazu, Chiba 292-0818, Japan[6]

*To whom correspondence should be addressed. Tel. +81 75-751-3291 (R.N.); +81 438-52-3913/+81 45-503-9696 (O.O.). Fax. +81 75-752-2361 (R.N.); +81 438-52-3914/+81 45-503-9694 (O.O.).
Email: rnishiko@kuhp.kyoto-u.ac.jp (R.N.); ohara@kazusa.or.jp/oosamu@rcai.riken.jp (O.O.)

Edited by Mitsuo Oshimura
(Received 18 November 2011; accepted 26 December 2011)

Abstract

Chronic infantile neurological cutaneous and articular syndrome (CINCA), also known as neonatal-onset multisystem inflammatory disease (NOMID), is a dominantly inherited systemic autoinflammatory disease and is caused by a heterozygous germline gain-of-function mutation in the *NLRP3* gene. We recently found a high incidence of *NLRP3* somatic mosaicism in apparently mutation-negative CINCA/NOMID patients using subcloning and subsequent capillary DNA sequencing. It is important to rapidly diagnose somatic *NLRP3* mosaicism to ensure proper treatment. However, this approach requires large investments of time, cost, and labour that prevent routine genetic diagnosis of low-level somatic *NLRP3* mosaicism. We developed a routine pipeline to detect even a low-level allele of *NLRP3* with statistical significance using massively parallel DNA sequencing. To address the critical concern of discriminating a low-level allele from sequencing errors, we first constructed error rate maps of 14 polymerase chain reaction products covering the entire coding *NLRP3* exons on a Roche 454 GS-FLX sequencer from 50 control samples without mosaicism. Based on these results, we formulated a statistical confidence value for each sequence variation in each strand to discriminate sequencing errors from real genetic variation even in a low-level allele, and thereby detected base substitutions at an allele frequency as low as 1% with 99.9% or higher confidence.

Key words: next generation sequencing; mosaicism; DNA diagnosis; chronic infantile neurological cutaneous and articular syndrome

1. Introduction

Chronic infantile neurological cutaneous and articular syndrome (CINCA; MIM #607115), also known as neonatal-onset multisystem inflammatory disease (NOMID), is a dominantly inherited autoinflammatory disease that is characterized by neonatal onset and a triad of symptoms, including an urticarial-like skin rash, neurological manifestations, and arthritis/arthropathy.[1–3] Patients often experience

† These authors contributed equally to this work.

recurrent fever and systemic inflammation. CINCA/NOMID is the most severe clinical phenotype in the spectrum of cryopyrin-associated periodic syndromes (CAPS), which also include two less severe but phenotypically similar syndromes, familial cold autoinflammatory syndrome (FCAS; MIM #120100), and Muckle–Wells syndrome (MWS; MIM #191900). CAPS are caused by mutations in the *NLRP3* gene, which is a member of the Nod-like receptor (NLR) family of the innate immune system.[4–6]

Approximately 60% of CINCA/NOMID patients carry heterozygous germline missense mutations in the *NLRP3* coding region (mutation-positive patients).[7] More than 80 different disease-causing mutations have been reported to date.[8] However, the remaining clinically diagnosed CINCA/NOMID patients (~40%) show no heterozygous germline *NLRP3* mutation based on conventional DNA sequencing-based genetic analyses (mutation-negative patients). In a previous international collaborative study, we found that there was a high incidence of somatic *NLRP3* mosaicism in mutation-negative CINCA/NOMID patients worldwide.[9] The level of mosaicism ranges from 4.2 to 35.8% (median = 10.2%). Rapidly diagnosing somatic *NLRP3* mosaicism is important to ensure proper treatment. However, the conventional approach used to identify somatic mosaicism of the *NLRP3* gene is time and labour intensive due to the subcloning of the *NLRP3* exon polymerase chain reaction (PCR) products, hereafter designated as amplicons, followed by capillary DNA sequencing of more than 100 subclones for each patient. Thus, this approach is not suitable to routinely diagnose somatic mosaicism of the *NLRP3* gene and additional labour and time will be required to reliably identify somatic mosaicism that occurs at a lower rate. The aim of the present study was to establish a new method that can be used to reliably diagnose somatic mosaicism using the *NLRP3* gene as a model. Massively parallel DNA sequencing (MPS) technology is an obvious method of choice to identify somatic mosaicism, and this approach has been already reported by other groups.[10–12] However, a well-known caveat of MPS is the high rate of sequencing errors, which cannot be disregarded when identifying low-level somatic mosaicism. To our knowledge, there have been no reports of a reliable method to discriminate MPS sequencing errors from somatic mosaicism with statistical confidence.

In this study, we first analysed the patterns of sequencing errors in *NLRP3* coding exons at a single-residue resolution by MPS using a Roche 454 GS-FLX sequencer and then constructed an error rate map for each base position in the *NLRP3* exons. Based on the error rate map, we could formulate a discrimination pipeline of somatic mosaicism from sequencing errors and thereby detect new somatic mosaicism in mutation-negative CINCA/NOMID patients, whose somatic mutations were subsequently confirmed by subcloning and Sanger sequencing. This approach can also be generally used to identify low-level somatic mosaicism in other genes.

2. Patients and methods

2.1. *Patients and DNA materials*

Patients were clinically diagnosed with CAPS by their referring physicians and the *NLRP3* gene was examined using the conventional Sanger sequencing method. DNA samples were obtained from Japanese *NLRP3* somatic mosaic patients ($n = 5$) who have been previously described,[9,13] CAPS patients ($n = 5$) with heterozygous *NLRP3* mutations, and healthy donors ($n = 50$). Genomic DNA samples from mutation-negative CINCA/NOMID patients ($n = 10$) were obtained from the National Institute of Health, Bethesda, USA. To generate DNA samples with no mosaicism, we constructed a set of subcloned plasmids containing each exon and its flanking intronic regions in the *NLRP3* gene from healthy donor genomic DNA using a Topo TA cloning kit (Invitrogen, San Diego, CA, USA). The cloned plasmids containing each exon and the flanking regions were validated by Sanger sequencing. Written informed consent was obtained from all the patients and their families. The study was approved by the ethical committees of Kyoto University and Kazusa DNA Research Institute and was conducted in accordance with the Helsinki Declaration.

2.2. *MPS of* NLRP3 *gene amplicons*

Genomic DNA samples were extracted from whole blood or peripheral blood mononuclear cells as previously described. We used a two-step PCR assay and pooled sample libraries for MPS. To cover the entire *NLRP3* coding exonic regions and flanking intronic regions, 14 amplicons were designed to be as long as an average read length for a 454 GS-FLX sequencer (up to 450 bases) and then amplified from each genomic DNA sample (Fig. 1A). The sequences of the PCR primers that were used to generate these 14 amplicons are provided in Supplementary Table S1. The upper and lower amplicon-specific primer sequences were flanked by common 15-base adapter sequences (TGTAAAACGACGGCC and GGAAA CAGCTATGAC for the upper and lower primers, respectively) at the 5′ end in order to fuse the primer-binding sequence for MPS in the second-step PCR. The first PCR amplifications were performed in 50-μl reactions using 30 ng of genomic DNA, 1× PrimeSTAR GXL buffer, 0.2 mM of each dNTP,

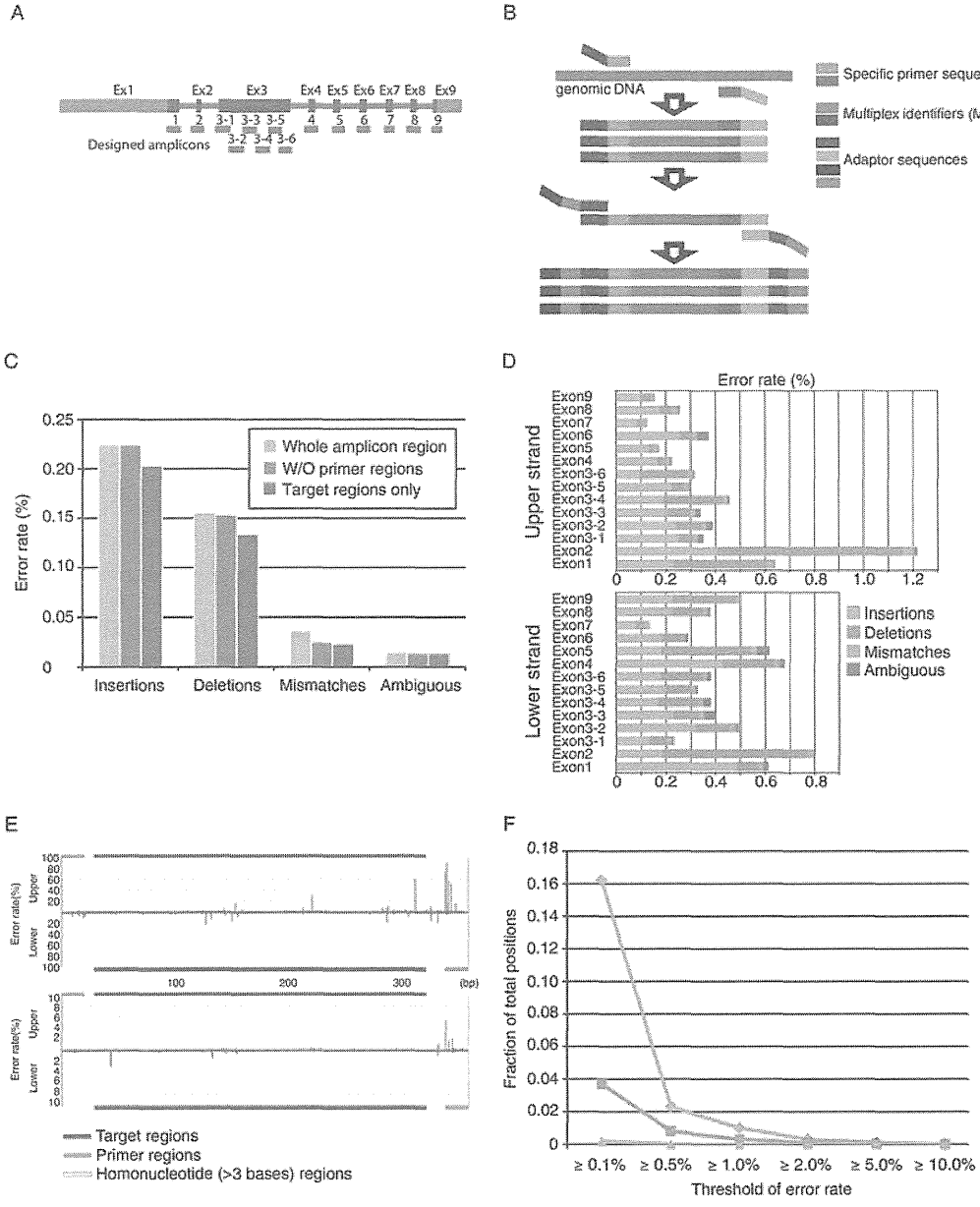

Figure 1. The amplicon analysis for *NLRP3* exons and its error rate. (A) Exon–intron structure of the *NLPR3* gene. Thick and thin rectangles depict exons and introns, respectively. Blue thick rectangles indicate the CDS region. The 14 designed amplicons (red) for nine exons are shown under the exon–intron structure. (B) Amplicon design schema. (C) Error rate for each error category in the region of entire amplicon (pale blue), that without designed primer regions (light blue), and the target regions (CDS + flanking intron; dark blue), respectively. (D) Strand-wise error rate for each amplicon. (E) Error rates along the amplicon sequence of exon 1 in each strand for insertions and deletions in the upper panel and mismatches and ambiguous base calls in the lower panel. The orange and blue lines depict the primer and target regions, respectively. The yellow shaded area depicts the homonucleotide ($n > 3$) region. The colour representation for the bars is the same as (D). (F) Co-occurrence error rate in both strands. The fraction of positions where a certain error occurred with the error rate for insertions, deletions, and mismatches. The colour representation is the same as in (D) and (E).

12.5 pmol of each forward and reverse primer, and 1.25 U of PrimeSTAR GXL DNA polymerase (Takara Bio, Shiga, Japan). The thermal cycling profile consisted of an initial denaturation step at 98°C for 1 min, followed by 28–32 cycles of 10 s denaturation at 98°C, 15 s of annealing at 60°C, and a 30 s extension at 68°C. The lengths of the PCR products ranged from 291 to 421 bp. The second PCR amplifications were performed using primers with adapter sequences at the 3′ end and Multiplex Identifier (MID) sequences at the 5′ end (Fig. 1B), which was used as a tag for each sample. The PCR reactions were performed in 50-μl volumes using 0.5 μl of the first PCR products, 1× PrimeSTAR GXL buffer, 0.2 mM of each dNTP, 12.5 pmol of each forward and reverse primer, and 1.25 U of PrimeSTAR GXL

DNA polymerase to attach the anchor sequences for MPS. The thermal cycling profile consisted of an initial denaturation step at 98°C for 20 s, followed by 20 cycles of 10 s denaturation at 98°C, 15 s of annealing at 60°C, and a 40 s extension at 68°C.

After confirming the amount and integrity of the PCR products by agarose gel electrophoresis, we mixed virtually equal amounts of the respective PCR amplicons that were generated using the same genomic DNA and applied the samples to a 454 Genome Sequencer (GS)-FLX system (Roche Diagnostics Corp., USA). All amplicons were amplified by emPCR and sequenced together in a multiplex fashion. MPS on this platform was performed as instructed by Roche. The sequencing reads from each of the pooled libraries were identified by their MID tags.

2.3. *Sequence data analysis*

The sequence read data were generated using GS RunProcessor ver.2.5.3 with default settings. Reads were sorted according to the MID tag sequences and were mapped to the reference amplicon sequences using the BLAT program[14] with the '-fine' option. In order to identify positions where the bases in a read differed from those in the reference sequence, each read was aligned to its reference sequence with the dpAlign module in the BioPerl package (http://www.bioperl.org/). The 454 pyrosequencing-related errors were categorized as insertions, deletions, mismatches, or ambiguous base calls. When aligning sequences, insertions/deletions are allocated based on the sequence context and strand orientation. To eliminate alignment artefacts due to insertion/deletion positions, the lower strand reads were converted to the reverse complement sequence, i.e. keeping the same strandness as the upper strand reads, when aligned with the reference sequence. A sequence error was defined as discordance in an equivalent position between the reference and control (from the 49 healthy individuals and a cloned plasmid vector). The error rate for a specified category was defined as the number of errors divided by the total number of bases in a read. The error rates of a base position on each strand were calculated from 50 control samples.

2.4. *Confirmation of somatic mosaicism of the* NLRP3 *gene by subcloning and subsequent capillary DNA sequencing*

To confirm the somatic mutational frequency that was identified based on the 454 sequencing data, we subcloned the PCR products and performed capillary DNA sequencing as previously described.[9] A Topo TA cloning kit (Invitrogen, San Diego, CA, USA) was used to subclone each of the 14 amplicons.

2.5. *Functional analysis*

To determine whether the identified *NLRP3* mutants are disease-causing, we assessed both ASC [apoptosis-associated speck-like protein containing a caspase recruitment domain; PYCARD, an approved symbol from the HUGO Gene Nomenclature Committee (HGNC) database]-dependent NF-κB activation in HEK293FT cells and transfection-induced cell death in THP-1 cells, a human monocytic cell line, as previously described.[9,13,15] cDNAs encoding carboxy-terminal green fluorescent protein (GFP)-tagged NLRP3 and its mutants were subcloned into pcDNA5/TO (Invitrogen). Before being introduced into THP-1 cells (10^6) using a Cell Line Nucleofector Kit V (Amaxa Biosystems, Cologne, Germany), phorbol myristate acetate (10 ng/ml) was added to enhance transient expression of *NLRP3* gene with minimizing spontaneous cell death.[15] Four hours after the introduction of plasmids (0.5 μg), cell death of GFP-positive THP-1 cells was measured by flow cytometry.

Expression plasmids for NLRP3 and ASC in the pEF-BOS vector background have been previously described.[13] HEK293FT cells (10^5) were transfected using TransIT-293 Transfection Reagent (Milus Bio, Madison, WI, USA) with an NF-κB reporter construct (pNF-κB-luc; 20 ng; BD Biosciences Clontech, Palo Alto, CA, USA), an internal control construct (pRL-TK; 5 ng; Toyo Ink, Tokyo, Japan), and wild-type or mutant NLRP3 expression plasmid (20 ng) in the presence or absence of ASC expression plasmid (20 ng). The amounts of total plasmid DNA used for transfection experiments were kept constant by adding pEF-BOS vector DNA. Twenty-four hours later, the transfected cells were harvested and subjected to dual luciferase assay by which the ability of each construct to induce NF-κB activation was assessed as previously described.[9]

3. Results

3.1. *Construction of base- and strand-specific error rate maps of* NLRP3 *exons from the MPS data of 50 control samples*

Errors in sequence reads generated by a Roche 454 GS-FLX sequencer are not randomly distributed along the sequence and depend on various factors.[16] Although this is a well-known characteristic of 454 sequencing, the occurrence pattern of these errors has not been explored in detail simply because these sequencing errors are considered noise that can be filtered out in most cases. However, it is highly critical to understand the occurrence pattern of sequencing errors on the MPS platform because low-level somatic mosaicism might appear at a rate close to that of sequencing errors. To address this, we collected

~1 million sequence reads using the 454 GS-FLX sequencer for 14 amplicons of *NLRP3* exons from 50 control samples that were thought to be free from somatic mosaicism, and ~94% of those reads were mapped to one of the reference *NLRP3* exon sequences. The number of sequencing depths for each amplicon of each sample on each strand was between 65 and 2139 (mean = 565.3, Supplementary Table S2). We found that the average error rate for each mutation category (insertion, deletion, mismatch, and ambiguous base calls) at each base position on each strand of the amplicons in the control samples was 0.22, 0.16, 0.036, and 0.014%, respectively (Fig. 1C). These values were consistent with those reported in a recent study on the error rates with 454 sequencing data.[16] The sequencing error in the 454 GS-FLX system tends to occur at the beginning and end of the reads,[11,16] and we confirmed this trend in our amplicon sequencing data (Supplementary Fig. S1). Moreover, after removing the end regions of the read sequences, we found that the error rates of the target regions for each category were 0.20, 0.134, 0.023, and 0.014%, respectively (Fig. 1C and Supplementary Table S3). When generating the amplicon sequences for the *NLRP3* exons, the target sequence (CDS region and flanking intron in 10-bp length) was designed to be 300−400 bp and not adjacent to primer sequences in order to obtain relatively low sequencing error rates (Fig. 1C). However, when the base- and strand-specific error rates of the respective amplicons were compared, we noticed that there were large variations in the error rate among amplicons in a strand-specific manner (Fig. 1D). We further examined the occurrence pattern of sequencing errors, as shown in Fig. 1E; the average sequencing error rates at each base in the 50 control amplicons are shown in a bar graph, where the bars in the upper or lower direction show the sequence error rates at the base position on the upper or lower strand of the amplicons, respectively. As evident in Fig. 1E, the error rates at most residues were low (<1%) with some hotspots for each type of error. Most of the insertion/deletion errors preferentially occurred at a homonucleotide region (yellow regions in Fig. 1E) as previously described,[17] but it was not always the case for all of homonucleotide regions. We could not find any tight relationship between other sequence patterns and the error rate. In addition, there was almost no position where sequencing errors occurred at a similar rate on both strands. This is more clearly shown in Fig. 1F, which indicates the numbers of positions with sequence variations in both strands that were higher than the threshold along the horizontal axis. These results indicate that the sequence errors can be discriminated from real genetic alterations when the sequence is read in both directions. However, it is important to keep in mind that PCR errors are not distinct from real genetic alterations. We did not observe any base substitution at a rate higher than 1% in our experiments (Fig. 1F), and the overall PCR error rate under MPS conditions was lower than 1% as long as a high-fidelity DNA polymerase was used to generate the amplicons.

Because Gilles *et al.*[16] recently reported that the occurrence of sequencing errors using the Roche 454 GS-FLX DNA sequencer depends on various factors, we first examined variations in the sequencing error rates of *NLRP3* exons among samples in the same run. For each mutation category, we found a similar trend in the error distribution rate in the amplicon sequences among the control samples (Supplementary Figs S2−S4). We confirmed that, for almost all residues, the error rate distributions among the 50 control samples fitted a Poisson distribution (data not shown). We next examined the run-to-run variation of the sequencing error rate for *NLRP3* exons. For this purpose, we performed an additional MPS run with seven amplicons (exons 3, 4, and 6) that were newly prepared and compared the number and positions of the sequencing errors between two independent sequencing runs. Out of 1993 base positions in the target regions, there was a low occurrence rate of mismatch errors in both runs and this seemed to fit a Poisson distribution. However, insertion/deletion errors (>1% error rate) were observed at ~100 base positions (<5% in the target regions) in each run, and only a half of these errors were shared between both runs (Table 1).

Table 1. Run-to-run variations in the error occurrence (>1% frequency)

Error category	Upper strand			Lower strand			All[a]
	First run	Second run	Overlap	First run	Second run	Overlap	
Insertions	63	73	42	76	96	52	10
Deletions	36	44	24	29	65	20	2
Mismatches	0	0	0	3	0	0	0
Ambiguous base calls	6	8	6	12	10	10	0

[a]The number of positions where the error rates in each category were commonly >1% for both strands in two independent runs.

This indicated that the occurrence of insertion/deletion errors was considerably affected by the run conditions (probably due to variations in the absolute signal strengths of pyrosequencing). Thus, as previously reported, the detection of insertion/deletion mutations by MPS on the 454 GS-FLX system was quite error-prone at least at a limited number of residues. However, the results also implied that false-positive mosaic mutations could be avoided by considering the sequencing data for both strands because these run-dependent insertion/deletion errors occur only in a single strand. Taken together, we conclude that the obtained sequence error map is stable and sufficiently robust to discriminate substitution sequencing errors from low-level mosaicism.

3.2. *Discrimination formula for detection of somatic mosaicism with statistical confidence*

We next examined known SNPs, known heterozygous mutations and somatic mosaic mutations of CAPS patients using MPS. All of these variations appeared on both strands at the expected allele frequencies as shown in Fig. 2, again indicating that filtering the strand-specific sequence variations is unlikely to eliminate real genetic variations.

Based on the experimentally observed sequencing errors with the 454 GS-FLX system described above, we established a discrimination formula to detect low-level somatic mosaicism as follows. In previous studies, the number of reads with the sequence error of a certain category in a sequence position was modelled based on the Poisson distribution with two parameters λ and k where the expected number of reads containing an error and the observed number of reads containing a sequence alteration, respectively, are as shown below[18]:

$$\mathrm{Pois}(k;\lambda) = \frac{\lambda^k e^{-\lambda}}{k!}. \qquad (1)$$

This model assumes that the error rate is constant across the different sequence regions but our data described above pointed out that the sequence error rate varies with the sequence content.[19] Thus, we introduced a position- and strand-specific error rate $q_{i,j,d}$ for a certain error category j in amplicon position i with strand d based on the sequencing data from 50 control samples. With the error rate $q_{i,j,d,}$ the upper probability (P) that the number of reads (R) with a certain sequence alteration of category j in position i is equal or greater than the number of observed reads r out of N reads with a sequenced direction d for an unknown sample was defined as:

$$P(R \geq r_{i,j,d} | \lambda_{i,j,d}) = 1 - \sum_{k=0}^{r-1} \frac{\lambda_{i,j,d}^k e^{-\lambda_{i,j,d}}}{k!}, \qquad (2)$$

where, $\lambda_{i,j,d} = N_{i,d} \times q_{i,j,d}$.

For the mismatch error rate, we did not consider the type of base substituted in an amplicon position in this study. We took $(1 - P)$ as a measure of the statistical confidence of the data and conventionally set a threshold of the statistical confidence to be 99.9%. In other words, if P-value was <0.001, the sequence alteration was considered to be a real sequence variation, not an error. For the final identification of real genetic variation with low-level somatic mosaicism, we determined that both of the P-values for the ith residue in the upper and lower strands must be smaller than the threshold.

To evaluate the lower detection limit for the allele frequencies of somatic mosaicism based on the statistical formulation shown above, we generated a series of known allele frequencies by diluting DNA from CAPS patients carrying heterozygous *NLRP3* mutations (c.1043C>T, c.1316C>T, and c.1985T>C) with DNA from normal donors carrying the wild-type *NLRP3* gene. In the dilution series, the mutant allele frequencies were adjusted to be 10, 5, 3, 2, 1, and 0.5% (Table 2). The data indicated that somatic mosaicism at these sites and at an allele frequency $\geq$1% could be convincingly detected with statistical significance ($P < 0.001$) if more than 350 reads for each strand were obtained for an amplicon. We also applied this statistical method to detect somatic mosaicism in patients with known low-level mosaic mutations described above and confirmed that all of

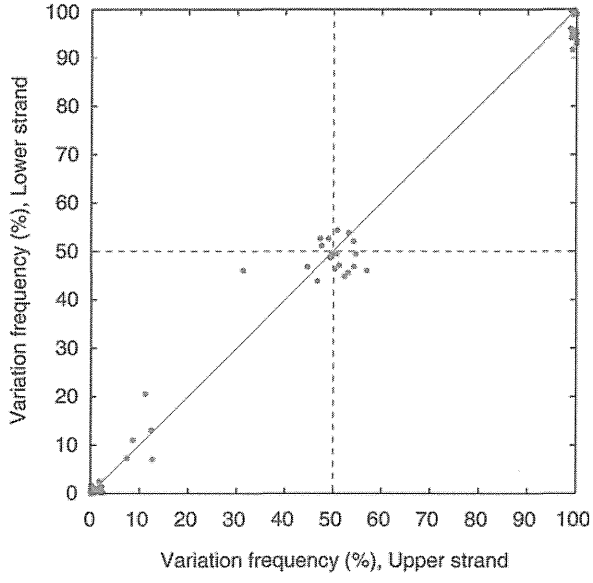

Figure 2. Scatter plot of the observed frequency variation in both strands. The colours depict known SNPs (green), heterozygous and mosaic mutations (orange) and errors (grey).

Table 2. *Evaluation of the lower detection limit for mosaicism with three sets of dilution series*

Mutation	Dilution (%)	Upper strand				Lower strand			
		Total reads	Mutant reads	%Mutant	*P*-value	Total reads	Mutant reads	%Mutant	*P*-value
c.1043C>T; p.Thr348Met	10.0	724	61	8.43	8.62E−130	520	57	10.96	1.73E−117
	5.0	453	24	5.30	2.86E−47	372	15	4.03	1.26E−25
	3.0	876	27	3.08	1.16E−46	757	21	2.77	6.83E−32
	2.0	737	10	1.36	1.05E−14	645	7	1.09	8.68E−09
	1.0	715	9	1.26	4.73E−13	624	4	0.64	1.11E−04
	0.5	1025	7	0.68	1.15E−14	756	3	0.40	3.22E−03[a]
c.1431C>A; p.Asn477Lys	10.0	542	65	11.99	1.22E−113	346	24	6.94	6.84E−49
	5.0	491	30	6.11	1.13E−44	356	17	4.78	2.42E−32
	3.0	487	21	4.31	1.26E−28	374	19	5.08	1.78E−36
	2.0	577	18	3.12	2.78E−22	495	9	1.82	4.57E−14
	1.0	491	4	0.82	9.17E−04	354	5	1.41	7.34E−08
	0.5	483	0	0	NA	424	3	0.71	NA
c.1985T>C; p.Met662Thr	10.0	658	79	12.01	1.13E−179	643	74	11.51	4.64E−167
	5.0	643	31	4.82	2.56E−59	608	33	5.43	9.96E−65
	3.0	777	27	3.48	4.65E−48	704	29	4.12	1.26E−53
	2.0	929	21	2.26	7.59E−34	835	15	1.80	3.92E−23
	1.0	735	17	1.09	2.74E−11	709	9	1.27	4.06E−13
	0.5	702	2	0.29	3.90E−03[a]	590	1	0.17	1.37E−01[a]

[a]Not significant.

Table 3. Potential mosaic mutations detected in patients with unknown mutations

Patient ID	Amplicon #	Variation		% Variation frequency		*P*-value		dbSNP	State
				Forward	Reverse	Forward	Reverse		
P1	Exon3_2	c.907G>C	p.Asp303His	7.12	11.56	3.0E−44	1.7E−84	rs121908153	Known
P2	Exon3_5	c.1699G>A	p.Glu567Lys	5.94	5.79	2.0E−69	8.9E−47	—	Known
P3	Exon3_5	c.1699G>A	p.Glu567Lys	18.28	15.33	0.0E+00	1.0E−312	—	Known
P4	Exon3_2	c.906C>A	p.Phe302Leu	9.78	9.70	1.7E−86	2.2E−122	—	Novel

the mutations could be detected with statistical significance without any false positives (data not shown).

3.3. *Detection and characterization of* NLRP3 *somatic mosaicism using the MPS platform*

To demonstrate the power of this approach in practice, we applied our new pipeline for 10 CINCA/NOMID patients in whom we failed to detect mutations in the *NLRP3* gene using a conventional direct DNA sequencing approach. The mutations detected by the analysis formulated using the MPS platform in this study are listed in Table 3. We successfully identified four out of the 10 patients with *NLRP3* somatic mosaicism, which was confirmed by subcloning and Sanger sequencing. The nucleotide substitutions were as follows (parentheses indicate the corresponding amino acid change): c.907G>C (p.Asp303His), c.1699G>A (p.Glu567Lys) in two patients, and c.906C>A (p.Phe302Leu). The frequencies of mosaicism identified in these patients by the MPS approach were consistent with those that were identified by the subcloning and subsequent capillary DNA sequencing method (data not shown). Both c.907G>C and c.1699G>A variants were reported as CINCA/NOMID-associated mutations in Infevers database (http://fmf.igh.cnrs.fr/ISSAID/infevers/) and in the dbSNP database (http://www.ncbi.nlm.nih.gov/projects/SNP/).[8]

Because the NLRP3 p.Phe302Leu mutation was novel and not detected in the 50 healthy controls, we performed an *in vitro* functional analysis to see the effect of p.Phe302Leu on the protein function. We used two different *in vitro* transfection experiments,

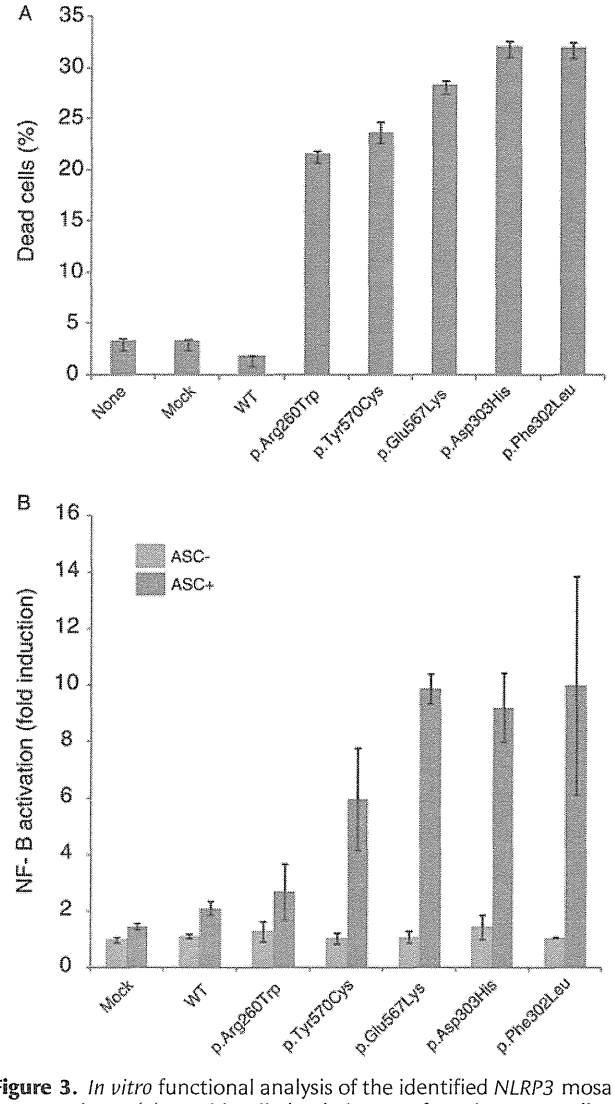

Figure 3. *In vitro* functional analysis of the identified *NLRP3* mosaic mutations. (A) Rapid cell death in transfected THP-1 cells. A GFP-fused wild-type or mutant *NLRP3* was transfected into THP-1 cells and incubated with PMA (10 ng/ml) for 4 h. The percentage of dead cells (7-amino-Actinomycin D [7-AAD]-positive) among the GFP-positive cells is shown. Data represent the means ± SD of triplicate experiments and are representative of two independent experiments. The data for previously reported mutations as well as the mutations found in this study are shown. (B) ACS-dependent NF-κB activation in transfected HEK293FT cells. HEK293FT cells were co-transfected with wild-type or mutant *NLRP3* in the presence or absence of ASC. NF-κB induction is shown as the fold-change compared with cells that were transfected with a control vector without ASC (set equal to one). Values are the means ± SD of triplicate experiments, and the data are representative of three independent experiments. The data for previously reported mutations (p.Arg260Trp and p.Tyr570Cys) and the mutations found in this study are shown. For each mutation, the data obtained in the presence and absence of ASC are shown. These findings identified p.Phe302Leu as a novel disease-causing mutation.

the rapid cell death in transfected THP-1 cells and the ASC-dependent NF-κB activation in transfected HEK293FT cells (Fig. 3A and B, respectively). Both assays clearly showed that p.Phe302Leu was a disease-causing mutation similar to known CINCA/NOMID-associated pathogenic mutations (p.Asp303His and p.Glu567Lys).[9]

4. Discussion

Although the somatic mutation rate at the nucleotide level *in vivo* was difficult to quantitatively measure due to the complexity of the genome and laborious molecular detection processes, recent advances in MPS technologies have allowed us to directly quantitate somatic mutations in human genome.[20–22] The current estimate for the somatic (*de novo*) mutation rate is $1-2 \times 10^{-8}$ residues/generation/haploid, and this estimate is sufficiently low that we would expect to never observe somatic mosaicism in the *NLRP3* gene by chance; although the error rate of the high-fidelity DNA polymerase used to produce the amplicons is two orders of magnitude larger than the somatic mutation rate,[23,24] we could not detect PCR-generated mosaicism higher than 1% in the 454 sequencing error maps. Based on the literature, the single base substitutions are the most frequent type of somatic mutations (~500 times more frequent than short insertions/deletions)[25] and protein-coding sequences are less mutagenic than sequences in non-coding regions, assuming that the somatic mutation spectrum in malignant cells is the same as in normal cells. Somatic mosaicism is thought to result from *de novo* gain-of-function-type mutations that are introduced at a very early and limited stage of development, and it is reasonable to focus our efforts on detecting base substitutions for somatic mosaicism in the *NLRP3* gene.

It is challenging but highly important in many areas of research, such as cancer, to detect low-level somatic mutations, which we designated as somatic mosaicism in this study, from apparently mutation-negative samples by conventional sequencing. Subcloning followed by the capillary DNA sequencing has been a *de facto* standard to identify somatic mosaicism, but this is not the method of choice for routine diagnostics because it is laborious, time consuming, and costly. Thus, it is reasonable for us to explore MPS as a new tool for this purpose. Although previous studies have used MPS technology to detect somatic mosaicism, it was unclear how sensitive this method is to detect a low-level somatic mosaicism using the MPS platform because this platform is generally error-prone. To address this challenge, we developed a new pipeline to detect low-level somatic mosaicism with statistical confidence using base position- and strand-specific error rate maps for the *NLRP3* amplicons to be studied. Whereas the

detection limit of somatic mosaicism depends on the base position and the read depth of the amplicons, the limit of detection could be as low as 1% allele frequency with no false positives for substitutions (the precision is higher than 99.9%). Our error map shows that 98.1% of base positions (3343 out of 3407 target positions) in the *NLRP3* exonic amplicons can be detected with ~1% mosaicism when more than ~350 reads were accumulated for each strand. Although the remaining region (64 base positions out of 3407 target positions) was too error-prone (the error rate ranged from 0.1 to 1.7% in either the upper or lower strand) to detect low-level mosaicism by MPS, medium-level mosaicism (5% or high) could be identified in all base positions in the target region with the same significance level. Based on this pipeline, we successfully identified four cases of somatic mosaicism among 10 apparently mutation-negative CINCA/NOMID patients. These results were subsequently confirmed by functional analysis and subcloning followed by capillary DNA sequencing method.

As described above, we revealed that a read depth of ~350 for each strand of each amplicon would be sufficient to detect somatic mosaicism as low as 1% with statistical confidence. This means that an analysis of somatic mosaicism (detection limit of 1% allele frequency) of the *NLRP3* gene for one sample requires $350 \times 2 \times 14 = 9800$ reads with the 454 GS-FLX sequencer, which has a capacity to obtain 1 000 000 reads per run. Thus, we could analyse ~100 patient samples with a single run (~10 h) using this MPS platform. For this purpose, a miniaturized 454 sequencer might be more convenient because it could analyse 10 patient samples at once with a reasonably reduced running cost.

The approach used to detect somatic mosaicism is very similar to that for low-frequency alleles in pooled DNA samples, for which MPS applications have been reported by many groups.[18,26,27] However, the main aim of these previous studies was to screen for a rare allele in a population. Thus, the discovery phase on the MPS platform must be followed by an evaluation phase using conventional methods. Therefore, when diagnosing somatic mosaicism of the *NLRP3* gene based solely on the MPS platform, we could not use the same approach to detect rare alleles in a population due to its low accuracy. The sequencing error rate on the Roche MPS platform was sufficiently stable and low enough as shown in this study. Using our pipeline, we were able to detect 1% somatic mosaicism in the *NLRP3* gene with 99.9% confidence. Although another research group recently used a similar approach with a short-read MPS,[28] the Roche long-read MPS is more suitable as a diagnostic tool mainly because of the short run time. If we could diagnose somatic mosaicism of the *NLRP3* gene within a reasonable time with low labour and costs as shown in this study, the success rate of CINCA/NOMID genetic diagnosis will increase from 60 to 80% or higher,[9] which will greatly advance the health and care of these patients and prevent irreversible bone and neurological complications of disease.

This pipeline would also be efficient to detect somatic mosaicism in mutation-negative patients with other diseases, including cancer. The error rate map for a given gene should be constructed from authentic plasmids, and used to detect somatic mosaicism of other genes as well as rare alleles in various populations.

Supplementary data: Supplementary data are available at www.dnaresearch.oxfordjournals.org.

Funding

This study was supported by the Japanese Ministry of Education, Science, Sports, and Culture, and the Japanese Ministry of Health, Labor, and Welfare.

Acknowledgements: We thank all patients who participated in the study. We are grateful to Ms. Yuki Takaoka at the Department of Pediatrics, Kyoto University Graduate School of Medicine and Mr. Takashi Watanabe at the Department of Human Genome Research, Kazusa DNA Research Institute for their technical assistance.

References

1. Prieur, A.M. and Griscelli, C. 1981, Arthropathy with rash, chronic meningitis, eye lesions, and mental retardation, *J. Pediatr.*, **99**, 79–83.
2. Hassink, S.G. and Goldsmith, D.P. 1983, Neonatal onset multisystem inflammatory disease, *Arthritis Rheum.*, **26**, 668–73.
3. Torbiak, R.P., Dent, P.B. and Cockshott, W.P. 1989, NOMID–a neonatal syndrome of multisystem inflammation, *Skeletal Radiol.*, **18**, 359–64.
4. Feldmann, J., Prieur, A.M., Quartier, P., et al. 2002, Chronic infantile neurological cutaneous and articular syndrome is caused by mutations in CIAS1, a gene highly expressed in polymorphonuclear cells and chondrocytes, *Am. J. Hum. Genet.* United States, 198–203.
5. Aksentijevich, I., Nowak, M., Mallah, M., et al. 2002, De novo CIAS1 mutations, cytokine activation, and evidence for genetic heterogeneity in patients with neonatal-onset multisystem inflammatory disease (NOMID)—a new member of the expanding family of pyrin-associated autoinflammatory diseases, *Arthritis Rheum.*, **46**, 3340–8.

6. Hoffman, H.M., Mueller, J.L., Broide, D.H., Wanderer, A.A. and Kolodner, R.D. 2001, Mutation of a new gene encoding a putative pyrin-like protein causes familial cold autoinflammatory syndrome and Muckle-Wells syndrome, *Nat. Genet.*, **29**, 301–5.
7. Goldbach-Mansky, R. 2011, Current status of understanding the pathogenesis and management of patients with NOMID/CINCA, *Curr. Rheumatol. Rep.*, **13**, 123–31.
8. Milhavet, F., Cuisset, L., Hoffman, H.M., et al. 2008, The infevers autoinflammatory mutation online registry: Update with new genes and functions, *Hum. Mutat.*, **29**, 803–8.
9. Tanaka, N., Izawa, K., Saito, M.K., et al. 2011, High incidence of NLRP3 somatic mosaicism in patients with chronic infantile neurologic, cutaneous, articular syndrome: results of an International Multicenter Collaborative Study, *Arthritis Rheum.*, **63**, 3625–32.
10. Qin, W., Kozlowski, P., Taillon, B.E., et al. 2010, Ultra deep sequencing detects a low rate of mosaic mutations in tuberous sclerosis complex, *Hum. Genet.*, **127**, 573–82.
11. Campbell, P.J., Pleasance, E.D., Stephens, P.J., et al. 2008, Subclonal phylogenetic structures in cancer revealed by ultra-deep sequencing, *Proc. Natl. Acad. Sci. USA*, **105**, 13081–6.
12. Rohlin, A., Wernersson, J., Engwall, Y., Wiklund, L., Bjoerk, J. and Nordling, M. 2009, Parallel sequencing used in detection of mosaic mutations: Comparison with four diagnostic DNA screening techniques, *Hum. Mutat.*, **30**, 1012–20.
13. Saito, M., Nishikomori, R., Kambe, N., et al. 2008, Disease-associated CIAS1 mutations induce monocyte death, revealing low-level mosaicism in mutation-negative cryopyrin-associated periodic syndrome patients, *Blood*, **111**, 2132–41.
14. Kent, W.J. 2002, BLAT—the BLAST-like alignment tool, *Genome Res.*, **12**, 656–64.
15. Fujisawa, A., Kambe, N., Saito, M., et al. 2007, Disease-associated mutations in CIAS1 induce cathepsin B-dependent rapid cell death of human THP-1 monocytic cells, *Blood*, **109**, 2903–11.
16. Gilles, A., Meglecz, E., Pech, N., Ferreira, S., Malausa, T. and Martin, J.F. 2011, Accuracy and quality assessment of 454 GS-FLX Titanium pyrosequencing, *BMC Genomics*, **12**, 245.
17. Margulies, M., Egholm, M., Altman, W.E., et al. 2005, Genome sequencing in microfabricated high-density picolitre reactors, *Nature*, **437**, 376–80.
18. Altmann, A., Weber, P., Quast, C., Rex-Haffner, M., Binder, E.B. and Muller-Myhsok, B. 2011, vipR: variant identification in pooled DNA using R, *Bioinformatics*, **27**, i77–84.
19. Dohm, J.C., Lottaz, C., Borodina, T. and Himmelbauer, H. 2008, Substantial biases in ultra-short read data sets from high-throughput DNA sequencing, *Nucleic Acids Res.*, **36**, e105.
20. Lee, W., Jiang, Z., Liu, J., et al. 2010, The mutation spectrum revealed by paired genome sequences from a lung cancer patient, *Nature*, **465**, 473–7.
21. Awadalla, P., Gauthier, J., Myers, R.A., et al. 2010, Direct Measure of the de novo mutation rate in Autism and Schizophrenia Cohorts, *Am. J. Hum. Genet.*, **87**, 316–24.
22. Conrad, D.F., Keebler, J.E.M., DePristo, M.A., et al. 2011, Variation in genome-wide mutation rates within and between human families, *Nat. Genet.*, **43**, 712–4.
23. Cha, R.S. and Thilly, W.G. 1993, Specificity, efficiency, and fidelity of PCR, *PCR Methods Appl.*, **3**, S18–29.
24. Vandenbroucke, I., Marck, H.V., Verhasselt, P., et al. 2011, Minor variant detection in amplicons using 454 massive parallel pyrosequencing: experiences and considerations for successful applications, *BioTechniques*, **51**, 167–77.
25. Pleasance, E.D., Cheetham, R.K., Stephens, P.J., et al. 2010, A comprehensive catalogue of somatic mutations from a human cancer genome, *Nature*, **463**, 191–6.
26. Fakhrai-Rad, H., Zheng, J.B., Willis, T.D., et al. 2004, SNP discovery in pooled samples with mismatch repair detection, *Genome Res.*, **14**, 1404–12.
27. Bansal, V. 2010, A statistical method for the detection of variants from next-generation resequencing of DNA pools, *Bioinformatics*, **26**, i318–24.
28. Flaherty, P., Natsoulis, G., Muralidharan, O., et al. 2012, Ultrasensitive detection of rare mutations using next-generation targeted resequencing, *Nucleic Acids Res.*, **40**, e2.

J Clin Immunol (2012) 32:221–229
DOI 10.1007/s10875-011-9629-0

Characterization of *NLRP3* Variants in Japanese Cryopyrin-Associated Periodic Syndrome Patients

Hidenori Ohnishi · Takahide Teramoto · Hiroaki Iwata · Zenichiro Kato · Takeshi Kimura · Kazuo Kubota · Ryuta Nishikomori · Hideo Kaneko · Mariko Seishima · Naomi Kondo

Received: 5 August 2011 / Accepted: 1 December 2011 / Published online: 24 December 2011

Abstract The etiology of cryopyrin-associated periodic syndrome (CAPS) is caused by germline gene mutations in NOD-like receptor family, pryin domain containing 3 (*NLRP3*)/cold-induced autoinflammatory syndrome 1 (*CIAS1*). CAPS includes diseases with various severities. The aim of this study was to characterize patients according to the disease severity of CAPS. Five Japanese patients with four kinds of gene variations in *NLRP3* were found and diagnosed as CAPS or juvenile idiopathic arthritis. Two mutations in *NLRP3*, Y563N and E688K, found in CAPS patients exhibit significant positive activities in the nuclear factor-κB reporter gene assay. Increased serum interleukin (IL)-18 levels were only observed in severe cases of CAPS. In mild cases of CAPS, the serum IL-18 levels were not increased, although lipopolysaccharide- or hypothermia-enhanced IL-1β and IL-18 production levels by their peripheral blood mononuclear cells were detectable. This series of case reports suggests that a combination of in vitro assays could be a useful tool for the diagnosis and characterization of the disease severity of CAPS.

Keywords Autoinflammatory disease · cryopyrin · familial cold autoinflammatory syndrome · interleukin-18 · *NLRP3*

Abbreviations

CAPS	Cryopyrin-associated periodic syndrome
CIAS1	Cold-induced autoinflammatory syndrome 1
CINCA	Chronic infantile neurologic cutaneous and articular
CRP	C-reactive protein
FCAS	Familial cold autoinflammatory syndrome
HEK	Human embryonic kidney
IL	Interleukin
JIA	Juvenile idiopathic arthritis
LPS	Lipopolysaccharide
MWS	Muckle–Wells syndrome
NLRP3	NOD-like receptor family, pryin domain containing 3
NF-κB	Nuclear factor-κB
NOMID	Neonatal-onset multisystem inflammatory disease
PBMCs	Peripheral blood mononuclear cells
TNF	Tumor necrosis factor

Introduction

Cryopyrin-associated periodic syndrome (CAPS) is an autoinflammatory syndrome [1] caused by germline gene mutations in NOD-like receptor family, pryin domain containing 3 (*NLRP3*)/cold-induced autoinflammatory syndrome 1 (*CIAS1*) [2–4]. The diagnosis of CAPS is based on its

H. Ohnishi (✉) · T. Teramoto · Z. Kato · T. Kimura · K. Kubota · H. Kaneko · N. Kondo
Department of Pediatrics, Graduate School of Medicine,
Gifu University,
1-1 Yanagido,
Gifu 501-1194, Japan
e-mail: ohnishih@gifu-u.ac.jp

H. Iwata · M. Seishima
Department of Dermatology, Graduate School of Medicine,
Gifu University,
Gifu, Japan

R. Nishikomori
Department of Pediatrics, Graduate School of Medicine,
Kyoto University,
Kyoto, Japan

H. Kaneko
Department of Clinical Research, Nagara Medical Center,
Gifu, Japan

characteristic clinical phenotypes and examination of gene mutations in *NLRP3*. A hotspot of gene mutations in *NLRP3* is located on exon 3. On the other hand, approximately 40% of cases with the clinically diagnosed severe form of CAPS, chronic infantile neurologic cutaneous and articular (CINCA)/neonatal-onset multisystem inflammatory disease (NOMID) syndrome, have no detectable germline gene mutations in *NLRP3* [5, 6]. Some of these patients have gene mutations in *NLRP3* outside of exon 3, *NLRP12*, or somatic mosaicism of *NLRP3* [5, 7–10]. In some of the remaining typical CAPS patients, the disease-causing mutations cannot be confirmed. Thus, the clinical phenotypes are very important for diagnosing CAPS patients.

Familial cold autoinflammatory syndrome (FCAS) shows the mildest clinical phenotypes in the spectrum of CAPS, such as cold-induced urticaria-like skin rash, while CINCA/NOMID syndrome shows additional severe phenotypes, such as severe arthritis, patella overgrowth, aseptic meningitis, mental retardation, and progressive sensory neural hearing loss [1]. The diagnosis of FCAS is relatively difficult owing to its mild phenotypes compared with the more severe phenotypes of CAPS (CINCA/NOMID syndrome or Muckle–Wells syndrome (MWS)). On the other hand, and similar to other autoinflammatory syndromes such as familial Mediterranean fever, it is important for CAPS treatment to prevent the onset of renal amyloidosis for consideration of the prognosis. Interleukin (IL)-1β inhibitory drugs, such as anakinra, rilonacept, and canakinumab, can prevent the clinical phenotypes of CAPS including renal amyloidosis [11]. However, the usage of IL-1 blockade for the severe form of CAPS may sometimes be an overtreatment for FCAS because the clinical symptoms are relatively mild and the frequency of onset of renal amyloidosis was reported to be low in FCAS patients [11]. Therefore, precise evaluation of the disease severity of CAPS may contribute to a reduction in the usage of IL-1 blockade. Consequently, a convenient objective standard is anticipated for discrimination between the mild and severe forms of CAPS.

In this study, to diagnose CAPS and characterize the differences between the mild and severe forms of CAPS, we evaluated the serum inflammatory cytokine levels, cytokine production levels by peripheral blood mononuclear cells (PBMCs), and cell-based nuclear factor (NF)-κB reporter gene activities of *NLRP3* variants in patients. Our results provide new insights into the characterization of the severity of CAPS.

Methods

Case Reports

The five clinical cases evaluated in this study are described below, and their characteristics are summarized in Table I.

Table I Genotypes and clinical profiles of the patients

	Analyzed age	Onset age	Gender	Diagnosis	Genotype (*NLRP3*)	CNS		Skin	Joint	Others		The inflammatory markers	
						Meningitis	Mental retardation	Urticaria like rash	Arthritis	Hearing loss	Renal amyloidosis	WBC (/μl)	CRP (mg/dl)
Case 1	3 months	3 months	Female	FCAS	Y563N	–	–	+	–	–	–	14,890	0.48
Case 2	34 years	Unknown	Male	FCAS	Y563N	–	–	+	+	–	–	13,120	3.05
Case 3	14 years	11 months	Male	CINCA/NOMID	E688K, G809S	+	+	+	+	–	–	22,500	12.30
Case 4	45 years	Unknown	Female	MWS	E688K	–	–	+	+	+	–	13,640	4.17
Case 5	3 years	3 years	Female	JIA	E378K	–	–	+	+	–	–	15,200	11.69

CNS central nervous system, *FCAS* familiar cold inflammatory syndrome, *CINCA* chronic infantile neurologic cutaneous and articular syndrome, *MWS* Muckle–Wells syndrome, *JIA* juvenile idiopathic arthritis, *WBC* the count of white blood cells, *CRP* the serum C-reactive protein level

All of the patients' family members and healthy control subjects provided informed consent to participate in the study, and the ethical principles of the Declaration of Helsinki were followed.

Case 1 The onset of disease (FCAS) in this patient occurred at 3 months of age. She exhibited a recurrent generalized urticaria-like skin rash upon exposure to cold temperatures (Fig. 1a). Progressive sensory neural hearing loss and renal amyloidosis were not seen. Her serum C-reactive protein (CRP) levels were continuously and slightly increased (0.24–2.1 mg/dl).

Case 2 Case 2 was the father of case 1. He was a 34-year-old male with a recurrent urticaria-like skin rash, fever, conjunctivitis, and arthralgia that developed following fatigue or exposure to cold temperatures. The precise time of his disease onset was unknown. Progressive sensory neural hearing loss and renal amyloidosis were not seen [12]. His CRP levels were continuously increased (1.52–3.98 mg/dl).

Case 3 The onset of disease (CINCA/NOMID) in this patient occurred at 11 months of age. Continuous aseptic meningitis, urticaria-like skin rash, arthritis at the end of the fingers, and Raynaud's symptoms were observed. Arteriosclerosis of the ophthalmic artery was found. However, severe patella overgrowth was not seen. At 14 years of age, he had heart failure with myocarditis, which was considered to be a rheumatic characteristic. The patient died suddenly at 19 years of age (the detailed clinical case will be described elsewhere by Teramoto et al.).

Case 4 Case 4 was the mother of case 3. The precise time of her disease (MWS) onset was unknown. Initially, she was diagnosed with rheumatic arthritis and received oral prednisolone therapy. She suffered progressive sensory neural hearing loss at 30 years of age and underwent artificial cochlea replacement therapy at 48 years of age. This was greatly effective in improving her hearing ability. Meningitis and renal amyloidosis were not seen.

Case 5 The onset of disease in this patient occurred at 3 years of age. Fever that continued for more than 2 weeks, severe polyarthritis (serum matrix metalloproteinase-3 of >800 ng/ml), and recurrent urticaria-like non-itchy skin rash (Fig. 1b) were observed. Lymphadenopathy, hepatosplenomegaly, and serositis were not seen. Patella overgrowth, aseptic meningitis, progressive sensory neural hearing loss, and renal amyloidosis were not seen. Rheumatoid factor was negative. Other autoantibodies, including anticyclic citrullinated peptide antibody, were not detected. Her serum CRP and ferritin levels were increased (11.69 mg/dl and 255.1 ng/ml, respectively). Based on the below-mentioned hereditary traits and the results of in vitro functional assays, we diagnosed this patient as juvenile idiopathic arthritis (JIA), according to the criteria for JIA from the International League of Associations for Rheumatology [13]. A combination therapy with steroid and tocilizumab was effective.

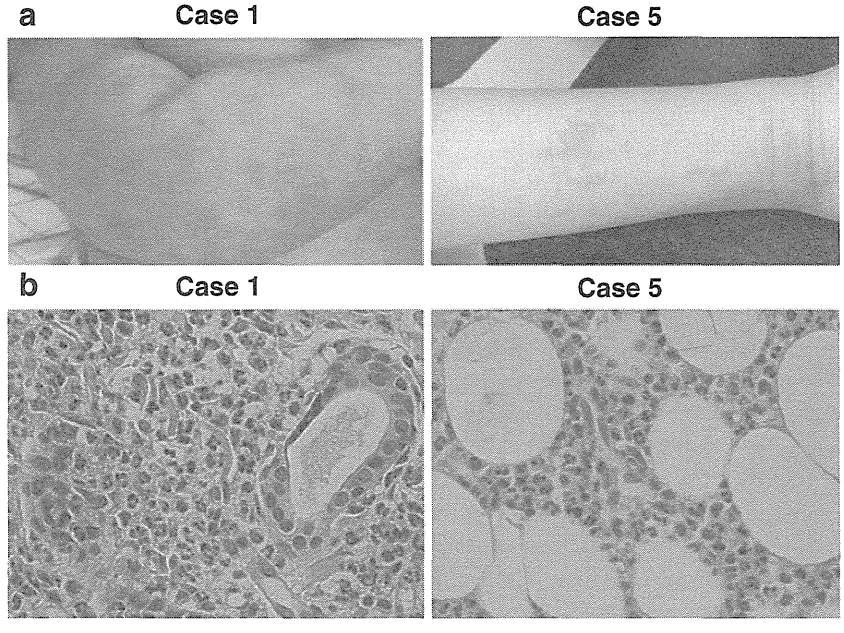

Fig. 1 Urticaria-like skin rash of cases 1 and 5. **a** Clinical appearances of the urticaria-like rash of cases 1 and 5. **b** Histopathological examinations of biopsy specimens from the skin rash of cases 1 and 5. Both skin biopsies show a recurrent cold-induced non-itchy urticaria-like skin rash and also show neutrophil infiltration

DNA Sequencing

Genomic DNA was extracted from leukocytes using Sepa-Gene (Eidia, Tokyo, Japan). A DNA fragment of the *NLRP3* gene was amplified by PCR and analyzed using Big Dye Terminator Bidirectional Sequencing (Applied Biosystems, Foster City, CA, USA).

Cell Culture

PBMCs were isolated from heparinized blood from control donors and patients by gradient centrifugation in Ficoll-Paque (GE Healthcare, Uppsala, Sweden). The PBMCs were cultured in medium consisting of RPMI 1640 supplemented with 10% heat-inactivated fetal calf serum, L-glutamine (2 mmol/l), penicillin (100 U/ml), and streptomycin (100 pg/ml). Human embryonic kidney (HEK) 293T cells were cultured in Dulbecco's modified Eagle's medium (high glucose-containing DMEM; Invitrogen, Carlsbad, CA, USA) supplemented with 10% heat-inactivated fetal bovine serum (Sigma-Aldrich, St. Louis, MO, USA), penicillin (100 U/ml), and streptomycin (100 μg/ml).

Vector Preparations

A cDNA encoding *NLRP3* tagged at the C terminus with a FLAG epitope (NLRP3-FLAG) was cloned into the plasmid vector pcDNA3.1+ (Invitrogen). Mutants of *NLRP3* (E378K, Y563N, E688K, and G809S) were generated using a GeneEditor In Vitro Site-Directed Mutagenesis System (Promega, Madison, WI, USA). An ASC variant 1 tagged at the C terminus with a myc epitope (ASC1-myc) was also cloned into pcDNA3.1+. An NF-κB luciferase reporter vector (pGL4.32-luc2P/NF-kappaB-RE/Hygro) and a *Renilla* luciferase reporter vector (pGL4.74-hRluc/TK) were purchased from Promega.

NF-κB Reporter Gene Activity

HEK293T cells in 96-well plates were transfected with 16 ng/well of pcDNA3.1+ control vector or pcDNA3.1+ NLRP3-FLAG vector (wild-type or mutant-type) using Lipofectamine 2000 (Invitrogen), according to the manufacturer's instructions. The pcDNA3.1+ ASC1-myc vector, NF-κB luciferase reporter vector, and *Renilla* luciferase reporter vector were cotransfected. After transfection, the cells were cultured for 24 h. The luciferase reporter gene activities were analyzed using a Dual-Luciferase Reporter Assay System (Promega). The statistical significance of differences in the luciferase activities between the wild-type and mutant genes in the NF-κB gene reporter assays was analyzed by the Kruskal–Wallis test, and further analysis was performed by the Bonferroni/Dunn test. Statistical significance was assumed for values of $P<0.05$.

Lipopolysaccharide- or Hypothermia-Induced Assays

PBMCs were suspended at 1×10^6 cells/ml in culture medium and cultured in the presence or absence of 10 or 100 ng/ml of LPSO127 (Sigma) for 24 h in six-well plates at 30°C or 37°C in a humidified atmosphere containing 5% CO_2.

Measurements of Tumor Necrosis Factor-α, IL-6, IL-1β, IL-1ra, and IL-18

Sera from the patients and healthy control subjects ($n=10$; age range, 1–35 years) were stored at −80°C until analysis. The sera of cases 1 and 2 were collected when they had the cold-induced rash, but not fever. The sera of cases 3, 4, and 5 were collected during a fever episode as an autoinflammatory symptom. Culture supernatants in test tubes or microtest plates were centrifuged to remove the cells and then stored at −80°C until analysis. The tumor necrosis factor (TNF)-α, IL-6, IL-1β, IL-1ra, and IL-18 concentrations were measured using a Human TNF-α Immunoassay Kit (BioSource, Camarillo, CA, USA), Human IL-6 Immunoassay Kit (BioSource), Human IL-1β Immunoassay Kit (BioSource), Quantikine Human IL-1ra/IL-1F3 ELISA Kit (R&D Systems, Minneapolis, MN, USA), and Human IL-18 ELISA Kit (MBL, Nagoya, Japan), respectively. The detection limits of the cytokine measurement kits were as follows: TNF-α, 1.7 pg/ml; IL-6, 2.0 pg/ml; IL-1β, 1.0 pg/ml; IL-1ra, 6.26 pg/ml; IL-18, 12.5 pg/ml. Values under the detection limits were shown as not detected. The serum cytokine levels were measured at two points at least, and the average values were calculated. The cytokine production levels by PBMCs were measured in duplicate and the average values were calculated. We defined cytokine levels of more than the mean+2 SD as increasing.

Results

Detection of Gene Variations in *NLRP3*

In the five patients, four heterozygous missense variations (E378K, Y563N, E688K, and G809S) of the *NLRP3* gene were identified (Table I). Interestingly, case 3 showed compound heterozygous gene variations, E688K and G809S, while his mother (case 4) had only one mutation, E688K, of *NLRP3*. The G809S allele was inherited from his asymptomatic father. In case 5, a novel missense variation, E378K, in *NLRP3* was identified. In addition, a heterozygous mutation, E148Q, in *MEFV* was identified. Gene mutations in *TNFRSF1A*, *MVK*, *NLRP12*, and *NOD2* were not found.

The genotypes of *NLRP3* and *MEFV* in her asymptomatic mother were the same. It should be noted that E378K and G809S were not present in the *INFEVERS* database (http://fmf.igh.cnrs.fr/ISSAID/infevers/) [14] and were confirmed as rare variants that were not identified in the 100 ethnically matched control subjects.

NF-κB Reporter Gene Activities of the *NLRP3* Variants

Figure 2 shows the ASC-dependent NF-κB activities of the *NLRP3* variants in vitro. The NF-κB reporter gene activities were increased by the Y563N and E688K mutations in *NLRP3*. The activities were higher for D303N (as a positive control *NLRP3* mutation that was previously identified in a CINCA/NOMID patient [5]) and E688K than for the FCAS mutation, Y563N. E378K and G809S did not cause any significant increases in the activities. Initially, we suspected that case 5 had CAPS. However, based on these results, we were able to confirm the diagnosis of case 5 as JIA, rather than CAPS.

Cytokine Profiles of the Patients

The serum IL-1β, IL-6, and TNF-α levels were not detected in the sera of the healthy control subjects. Although we were unable to detect IL-1β in the patients' sera, we clearly detected the serum IL-18 and IL-1ra levels in all cases (Fig. 3a, b). The serum IL-18 levels were extremely high in the CINCA/NOMID (case 3), MWS (case 4), and JIA (case 5) patients compared with the control subjects. The serum IL-1ra and IL-6 levels were increased in cases 2, 3, 4, and 5 (Fig. 3b, c). The serum TNF-α levels were increased in cases 1, 2, and 3 (Fig. 3d).

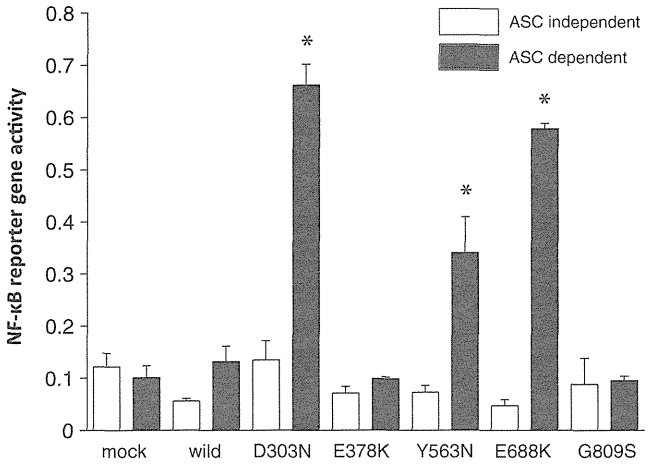

Fig. 2 NF-κB reporter gene activities of the *NLRP3* variants. The *white bars* indicate the NF-κB reporter gene activities of the *NLRP3* variants without cotransfection of ASC, while the *black bars* indicate these activities with cotransfection of ASC. The data shown are the means±SD of triplicate assays. The ASC-dependent NF-κB reporter gene activities are increased for the variants with D303N, Y563N, and E688K. The activities for the CINCA/NOMID mutations, D303N and E688K, are higher than those for the FCAS mutation, Y563N. The variants with E378K and G809S do not show any significant increases in the activities. *$P<0.05$

Interestingly, the serum IL-18 levels in the FCAS patients (cases 1 and 2) did not show any increases compared with the control subjects (Fig. 3a). Furthermore, the levels of spontaneous IL-1β production by PBMCs from the CINCA/NOMID (case 3) and MWS (case 4) patients were increased, whereas those of the control subjects, FCAS patients, and JIA patient (cases 1, 2, and 5) did not show any increases (Fig. 4a).

The lipopolysaccharide (LPS)-induced cytokine production levels by PBMCs from the FCAS and JIA patients are shown in Fig. 4b–d. The IL-1β and IL-18 production levels were increased in the FCAS patients compared with the control subjects. However, TNF-α did not show any significant changes. Comparisons of the cytokine production levels by the PBMCs cultured at 30°C and 37°C are shown in Fig. 5. The PBMCs from the FCAS patients showed obvious increases in the IL-1β and IL-18 production levels after culture at the lower temperature with no stimulation.

Discussion

The diagnosis of CAPS is still based on the clinical symptoms and recognition of a syndrome. Detection of a pathogenic *NLRP3* mutation can confirm the CAPS diagnosis. However, to confirm the diagnosis of CAPS patients with novel identified *NLRP3* variations, some functional experiments regarding the effects of the *NLRP3* mutations, such as the NF-κB luciferase reporter gene assay used in this study, are necessary because of the existence of nonfunctional missense variations of *NLRP3* [7]. Furthermore, although there are many previously reported missense mutations of *NLRP3* associated with CAPS in the *INFEVERS* database [14], the mutations with confirmed functional evidence are limited. In this study, we identified *NLRP3* gene mutations in five patients who were suspected of having autoinflammatory syndromes. Two mutations of *NLRP3*, Y563N and E688K, were previously reported to be disease-causing mutations [15, 16], although in vitro functional assays were not performed. Y563N was first identified in FCAS patients who were diagnosed based on the clinical criteria of FCAS [16, 17]. Our FCAS patients (cases 1 and 2) showed a skin rash, occasional fever, and mild arthritis and did not show any severe symptoms, such as neurological disorders, hearing loss, and renal amyloidosis. On the other hand, E688K was first identified in an Italian male CINCA/NOMID patient [15] who was described as having a skin rash, hearing loss, fever, and transient arthritis without persistent deformities of the involved joints. Our patients with E688K

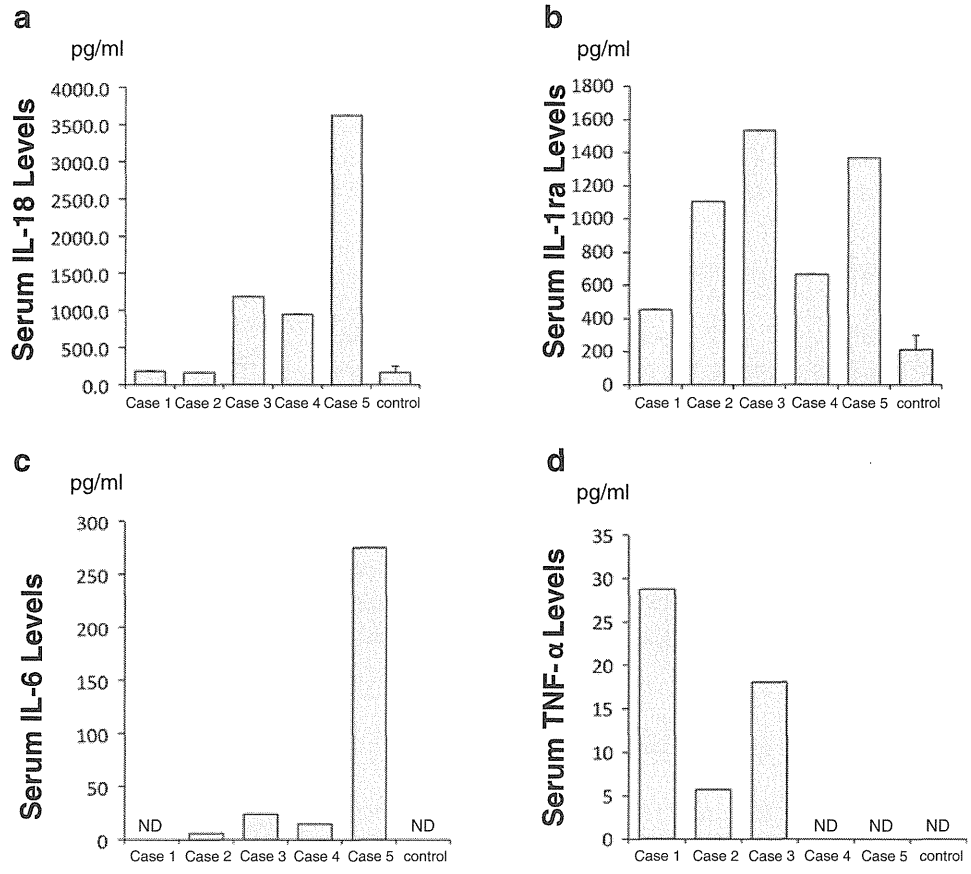

Fig. 3 Serum inflammatory cytokines in the four CAPS cases. IL-1β, IL-6, and TNF-α were not detected in the sera of the control subjects. The means ±D of the serum IL-18 and IL-1ra levels of the healthy control subjects were 169.2±85.7 and 213.4±87.1 pg/ml, respectively (n=10)

(cases 3 and 4) also had no strong deformities of the joints, but had obviously more severe phenotypes than FCAS, such as aseptic meningitis and hearing loss. In the present study, the E688K mutation in the MWS and CINCA/NOMID syndrome patients showed significantly stronger NF-κB activities than the Y563N mutation identified in the FCAS patients. Our findings indicate that the clinical phenotypes and values of the ASC-dependent NF-κB activity assay are well correlated with the genetic mutations, consistent with a previous report [18]. However, the artificial reporter gene assay system used may have little to do with the function of the CAPS pathophysiology, and limited numbers of *NLRP3* variants have been assessed using the assay in the present and previous studies, thereby making it difficult to prove this hypothesis at the present time. Consequently, further experiments including large amounts of pathogenic mutations and accumulation of detailed clinical information about the disease severity of CAPS are necessary to confirm this hypothesis. It should be noted that low-penetrance mutation, G809S, did not show positive activity with this in vitro assay system. But the clinical phenotype of case 3 was obviously more severe than case 4, although the father of case 3, who also was found to have G809S, was as symptomatic. Because of the discrepancy between the patient and the father, it remains unclear whether G809S is a pathogenic mutation or, alternatively, if there is an alternative genetic explanation for disease in the patient not detected by genomic DNA sequencing.

On the other hand, it requires time to build the above-mentioned in vitro experimental system. For the rapid diagnosis and characterization of CAPS, a simple screening system is necessary. In this study, we measured several serum inflammatory cytokine levels in our patients (Fig. 3). The serum IL-6 level is usually used for evaluating the disease severity of rheumatoid arthritis [19]. Moreover, the serum IL-18 level was recently reported to reflect the disease severity of not only JIA but also other diseases such as allergic diseases [20, 21]. In our CAPS patients, the serum levels of IL-18, but not IL-1β, seemed to be correlated with the disease phenotypes. Although the precise reason for this dissociation between the IL-18 and IL-1β levels in the sera is unknown, IL-1β may be rapidly neutralized, metabolized, or captured by a plethora of IL-1 receptors in vivo. In fact, serum IL-1ra, which is the counter-regulator of IL-1, was increased in our CAPS patients. Thus, the serum IL-18 levels may be used as an appropriate marker for the evaluation of treatments, although it is unlikely that serum IL-18 can contribute to the differential diagnosis between CAPS and other diseases.

The diagnosis of FCAS seems to be relatively difficult because of its mild phenotypes compared with the other more severe phenotypes of CAPS. The serum inflammatory

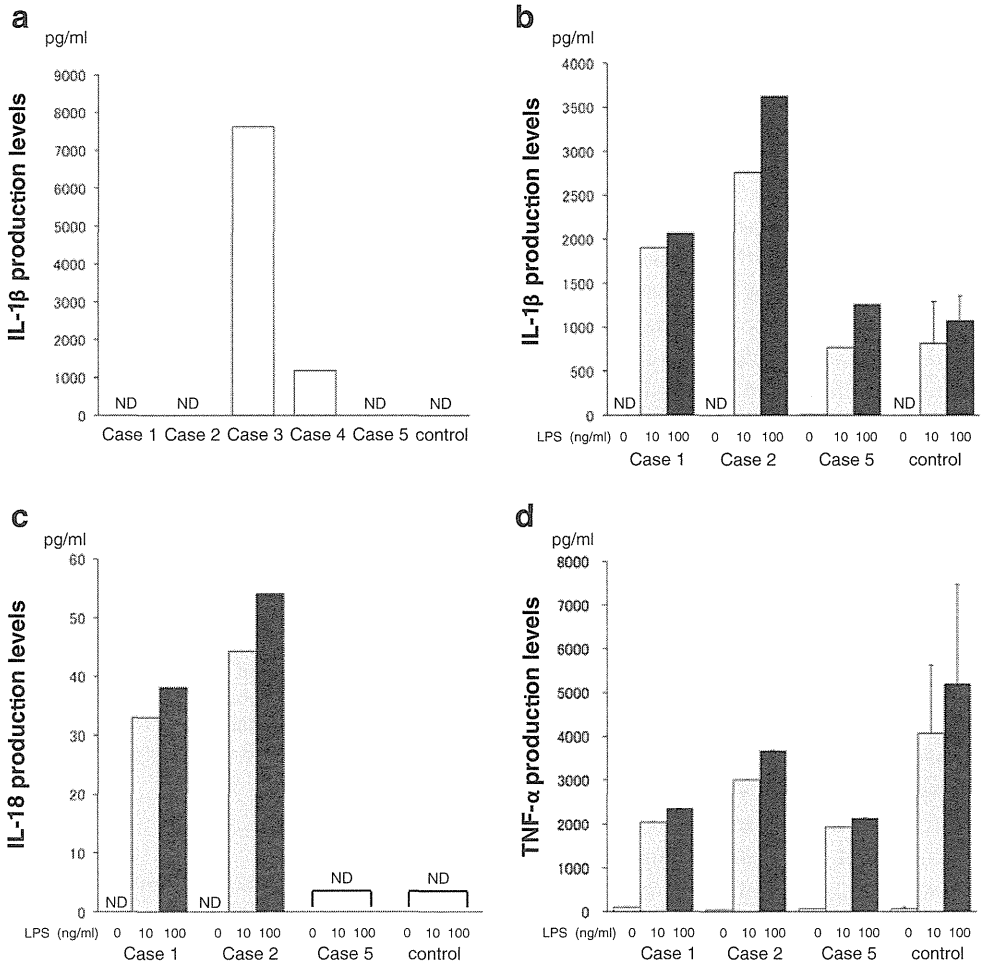

Fig. 4 LPS-induced cytokine production levels in the patients. **a** The *white bars* indicate the spontaneous IL-1β production levels by PBMCs. Increased IL-1β production by PBMCs from case 3 (CINCA/NOMID syndrome) and case 4 (MWS) is detected, whereas no increases are observed for the PBMCs from the control subjects and cases 1, 2 (FCAS), and 5 (JIA). **b**, **c** The LPS-induced IL-1β and IL-18 production levels by PBMCs from the FCAS patients are increased compared with PBMCs from the control subjects. **d** The TNF-α production levels by PBMCs from the FCAS and JIA patients do not show any significant changes. In **b**–**d**, the *white bars* indicate the cytokine production levels without stimulation and the *gray* and *black bars* indicate the cytokine production levels after stimulation by 10 and 100 ng/ml LPS, respectively

cytokine levels in our FCAS patients did not show any typical increases, unlike the case for the CINCA/NOMID patient (Fig. 3), indicating that the establishment of an effective and easy screening method is important for the diagnosis of FCAS. Therefore, we focused on the cytokine production levels in these patients' blood cells. First, IL-1β production by nonstimulated PBMCs was observed in our CINCA/NOMID and MWS patients (cases 3 and 4, respectively), as reported previously [5]. However, no enhancement of spontaneous IL-1β production was observed in our FCAS patients (cases 1 and 2) (Fig. 4a), suggesting that this method may not be suitable for screening of FCAS.

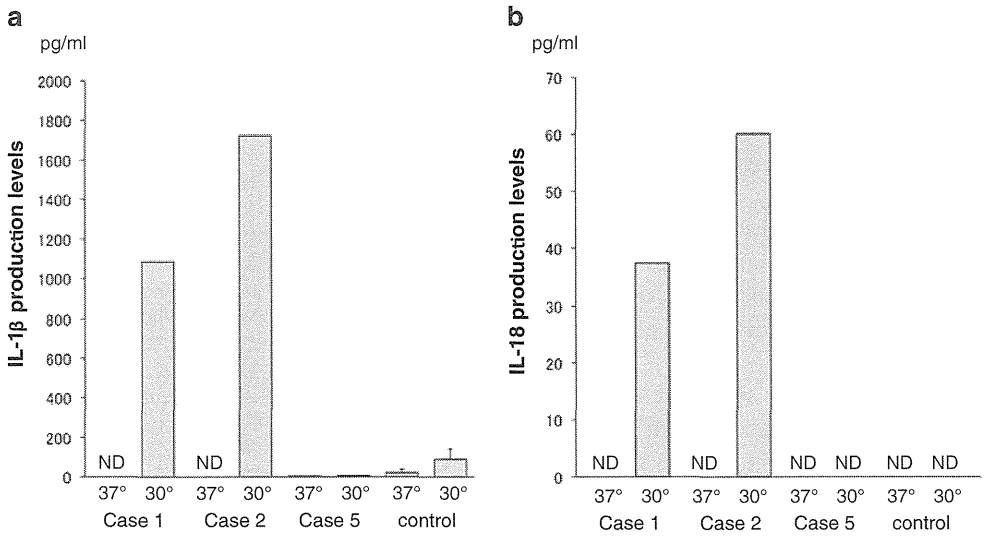

Fig. 5 Hypothermia-induced cytokine production levels by PBMCs from the FCAS and JIA patients. **a**, **b** Comparisons of the cytokine production levels by PBMCs cultured at 30°C and 37°C. The PBMCs from the FCAS patients (cases 1 and 2) show obvious increases in the IL-1β and IL-18 production levels after culture at lower temperature with no stimulation

Furthermore, the LPS- or hypothermia-induced cytokine production levels by the PBMCs showed marked elevation of IL-1β or IL-18 (Figs. 4a–c and 5b), as reported previously [16, 22]. The phenomena for hypothermic culture were similar to the findings in our recent report that NF-κB activity induced by LPS stimulation through TLR4 is enhanced in low-temperature cultures [23], although the precise mechanism of the association between the *NLRP3* variations and the low-temperature stimulation requires further clarification. These findings suggest that the cytokine production assays induced by LPS or hypothermia stimulation should be helpful for the diagnosis of FCAS. It should be noted that the serum IL-18 levels could be detected in all of the non-CAPS subjects, although the production levels of IL-18 from their PBMCs were lower than the detection limit. This might be dependent on the long half-life of IL-18 in human blood compared with the above-mentioned half-life of IL-1β.

The discrimination between CAPS and JIA cases is sometimes difficult because of their similar clinical characteristics. Interestingly, although case 5 had a rare missense variation in *NLRP3* (E378K) and some of her clinical symptoms were similar to those of CAPS (Table I), the E378K variant did not show enhancement of NK-κB activity (Fig. 2). This gene variation was inherited from her mother who did not show any inflammatory symptoms. Case 5 showed strong polyarthritis, continuous fever, and a recurrent generalized urticaria-like erythema as well as symptoms of CAPS. In particular, histopathological examination of a biopsy specimen from her skin rash revealed infiltration of neutrophils and mononuclear cells, representing similar findings to case 1 (Fig. 1). Thus, it was difficult to discriminate CAPS by the clinical symptoms alone in this case.

Therefore, to discriminate between CAPS and JIA in this case, we focused on her cytokine profiles. Her serum IL-6 and IL-18 levels were extremely high compared with not only the healthy controls but also the other CAPS patients (Fig. 3a, c). These observations resembled the serum cytokine pattern of systemic-onset JIA [21, 24]. Furthermore, the LPS-induced and hypothermia-induced IL-1β and IL-18 production levels by PBMCs from case 5 showed no increases compared with the control subjects (Figs. 4b, c and 5a, b). Recently, Saito et al. [5] reported that another screening method, LPS-induced monocyte cell death, was effective for diagnosing CAPS. The monocytes in case 5 did not show LPS-induced cell death. These objective results also supported the diagnosis of case 5 as JIA, rather than CAPS.

In this study, we evaluated several methods for the limited genotypes of patients with *NLRP3* variants. According to comparisons of the clinical phenotypes of previous case reports and our cases, the disease severity seems to be correlated with the serum cytokine levels and the ex vivo and in vitro responses and is almost completely determined by the specific mutations, which appear to suggest that other genetic or epigenetic determinants or environmental factors do not play a significant role.

Conclusions

A precise and easy method for the diagnosis of CAPS has not yet been established. The characteristics of the clinical phenotypes and the identification of proven gene variations of *NLRP3*, as the etiology of CAPS, are very important for diagnosing CAPS. In addition, the serum IL-18 levels and NF-κB activities of patients with the *NLRP3* variants reflect the phenotypes of disease severity. Evaluation of the cytokine profile is also a useful tool for diagnosing and discriminating the severity of CAPS.

Acknowledgements We thank the members of the families who agreed to participate in the study. We thank Dr. T. Fukao, Dr. M. Kawamoto, Dr. N. Kawamoto, and K. Kasahara for their advice and technical help. This work was supported by Grants-in-Aid for Scientific Research from the Ministry of Education, Science and Culture of Japan and by Health and Labour Science Research Grants for Research on Intractable Diseases from the Ministry of Health, Labour and Welfare.

Conflicts of Interest The authors have declared no conflicts of interest.

References

1. Hoffman HM, Simon A. Recurrent febrile syndromes: what a rheumatologist needs to know. Nat Rev Rheumatol. 2009;5:249–56.
2. Aksentijevich I, Nowak M, Mallah M, Chae JJ, Watford WT, Hofmann SR, et al. De novo CIAS1 mutations, cytokine activation, and evidence for genetic heterogeneity in patients with neonatal-onset multisystem inflammatory disease (NOMID): a new member of the expanding family of pyrin-associated autoinflammatory diseases. Arthritis Rheum. 2002;46:3340–8.
3. Feldmann J, Prieur AM, Quartier P, Berquin P, Certain S, Cortis E, et al. Chronic infantile neurological cutaneous and articular syndrome is caused by mutations in CIAS1, a gene highly expressed in polymorphonuclear cells and chondrocytes. Am J Hum Genet. 2002;71:198–203.
4. Hoffman HM, Mueller JL, Broide DH, Wanderer AA, Kolodner RD. Mutation of a new gene encoding a putative pyrin-like protein causes familial cold autoinflammatory syndrome and Muckle–Wells syndrome. Nat Genet. 2001;29:301–5.
5. Saito M, Nishikomori R, Kambe N, Fujisawa A, Tanizaki H, Takeichi K, et al. Disease-associated CIAS1 mutations induce monocyte death, revealing low-level mosaicism in mutation-negative cryopyrin-associated periodic syndrome patients. Blood. 2008;111:2132–41.
6. Tanaka N, Izawa K, Saito MK, Sakuma M, Oshima K, Ohara O, et al. High incidence of NLRP3 somatic mosaicism in chronic infantile neurological cutaneous and articular syndrome patients: the